SLAC-PUB-6378
October 1993

A Measurement of the LPM Effect

S.R. Klein et al.

Stanford Linear Accelerator ***Center,***
Stanford University, Stanford, CA 94309

Presented at the 6th International Symposium on Lepton and Photon Interactions, Cornell University, Ithaca, NY, August 10-15, 1993

Work supported by Department of Energy contract DE–AC03–76SF005 15.

SLAC–PUB–6378
November 1993
(T/E)

A MEASUREMENT OF THE LPM EFFECT*

S.R. Klein[a], P. Anthony[b,c], R. Becker-Szendy[c], P.E. Bosted[d], M. Cavalli-Sforza[a], L.P. Keller[c], L.A. Kelley[a], G. Niemi[c], M.L. Perl[c], L.S. Rochester[c], J. White[d]

[a] *Santa Cruz Institute for Particle Physics, University of California, Santa Cruz, Santa Cruz, CA, 95064*

[b] *Lawrence Livermore National Laboratory, Livermore, CA, 94550*

[c] *Stanford Linear Accelerator Center, Stanford University, Stanford, CA, 94305*

[d] *The American University, Washington D.C., 20016*

We have performed an experiment to measure accurately the Landau-Pomeranchuk-Migdal (LPM) effect in the production of 5 to 500 MeV photons due to bremsstrahlung of 8 and 25 GeV electron beams traversing thin (2 to 6% X_0) targets of varying densities. Our measurements confirm that the LPM effect exists and that the Migdal calculations are accurate. We see that, for thin targets, LPM suppression disappears leaving a Bethe-Heitler spectrum, as predicted by theory. For intermediate target thicknesses, we lack an acceptable theory, but have measured energy spectra for targets of differing thickness.

We have also measured the production rate of 500 keV to 5 MeV photons at the same electron energies, to study dielectric suppression. We see qualitative agreement with the theory of Ter-Mikaelian; more work is needed before we can make quantitative comparisons.

I. INTRODUCTION

In the early 1950s, a group of Russian theorists led by Landau, Pomeranchuk, Migdal, and Feinberg realized that because of the low longitudinal momentum transfer between the nucleus and the electron, bremsstrahlung is not really a point interaction, but occurs over a finite formation zone. While the electron traverses this formation zone, external influences can perturb the electron and suppress or enhance the photon emission, causing the traditional Bethe-Heitler (BH) formulae to fail. A well known example of this is crystal channeling, where photon emission by bremsstrahlung can be enhanced. Another example, discussed below, is the suppression of low-energy photons when the photon energy becomes comparable to the electron gamma times the plasma frequency of the media. A third example is the suppression of bremsstrahlung when multiple scattering disrupts the electron trajectory; this is known as the Landau-Pomeranchuk- Migdal (LPM) effect, after its discoverers.

Initially, Landau and Pomeranchuk used semiclassical arguments to determine that multiple scattering can change the $1/\omega_\gamma$ photon spectrum to $1/\sqrt{\omega_\gamma}$ [1]. Migdal later used scattering theory to quantify the effect more fully [2].

*Work supported by Department of Energy contracts DE–AC03–76SF00515 (SLAC) and W–4705–ENG–48 (LLNL) and National Science Foundation grants NSF–PHY–9113428 (UCSC) and NSF–PHY–9114958 (American).

Invited talk presented at the 16th International Symposium on Lepton and Proton Interactions Ithaca, NY, August 10–15, 1993

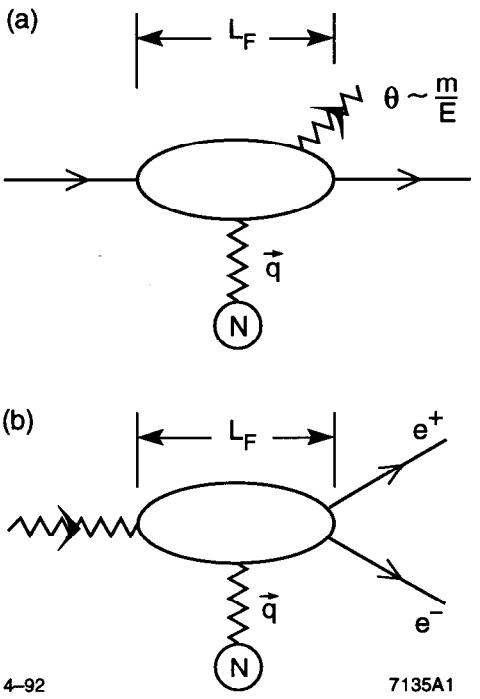

FIG. 1. Diagrams for (a) bremsstrahlung and (b) pair production, showing the formation zone.

Because Migdal's derivation is mathematically involved, we will present here a semiclassical derivation of Feinberg and Pomeranchuk [3].

The classical diagram for bremsstrahlung is presented in Fig. 1. An electron emits a photon, conserving momentum by exchanging a virtual photon with a nearby nucleus. The transverse momentum exchanged with the nucleus is up to the mass of the electron, m. However, the longitudinal momentum transfer is much smaller,

$$q_{\|} = p_e - p'_e - k = \sqrt{E_e^2 - m^2} - \sqrt{E_e'^2 - m^2} - E_\gamma,$$

where p_e, p'_e, E_e, and E'_e are the electron momentum and energy before and after the interaction, respectively, and E_γ is the photon energy. For high-energy electrons this simplifies to

$$q_{\|} \sim \frac{m^2 E_\gamma}{2E_e(E_e - E_\gamma)} \sim \frac{E_\gamma}{2\gamma^2},$$

where γ is E_e/m, and the latter relationship only holds for $E_\gamma \ll E_e$.

This momentum transfer can be very small. For example, for a 25 GeV electron emitting a 100 MeV photon, $q_{\|}$ is only 0.02 eV/c. Then, by the uncertainty principle, the virtual photon exchange distance is finite, $c\gamma^2/\omega_\gamma$. For a 100 MeV photon from a 25 GeV electron, the formation zone is 10μm long.

The LPM effect comes into play when one considers that the electron must be undisturbed while it traverses this distance. One factor that can disturb the electron, and suppress the bremsstrahlung, is multiple Coulomb scattering. If the electron multiple scatters by an angle θ_{MS}, greater than the emission angle of the bremsstrahlung photon, $\theta_B \sim m/E_e = 1/\gamma$, then the bremsstrahlung is suppressed.

One parameterization for multiple scattering is

$$\bar{\theta}^2_{MS} = (\frac{E_s}{E_e})^2 \frac{l}{X_0},$$

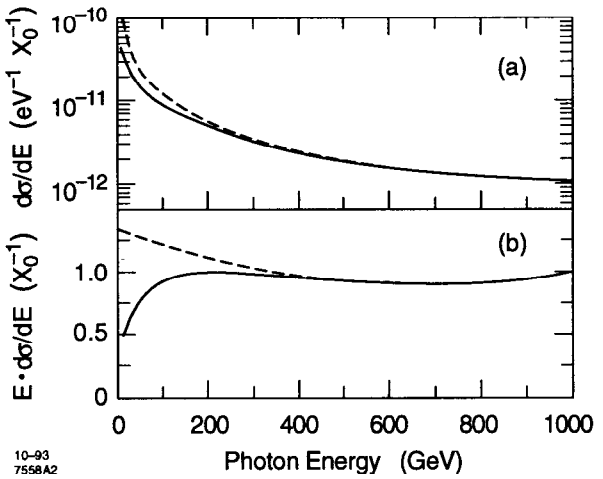

FIG. 2. (a) $d\sigma/dE_\gamma$ and (b) $E_\gamma \times d\sigma/dE_\gamma$ for bremsstrahlung from 1 TeV electrons in uranium for the BH and LPM formulae.

where E_s is the characteristic energy, $\sqrt{4\pi/\alpha} \cdot m_e = 21$ MeV, l is the target thickness, and X_0 is the radiation length. The above formula is inaccurate for thin media, where single large scatters can contribute significantly to the total scattering; Migdal's analysis considers this in more detail. The LPM effect becomes important when θ_{MS} is larger than θ_B. This occurs for $E_s/E_e\sqrt{x/X_0} > m/E_e$. Some algebra shows that for a given electron energy, suppression becomes significant for photon energies below a certain value, given by

$$x = \frac{E_\gamma}{E_e} < \frac{E_e}{E_{LPM}},$$

where all of the constants have been lumped into E_{LPM}, given by $E_{LPM}(\text{eV}) = m^4 X_0/c\hbar E_s^2 = 7.6 \times 10^{12} X_0(\text{cm})$, about 2.6 TeV in uranium and 4.2 TeV in lead. For example, suppression becomes significant for 250 MeV photons from a 25 GeV electron in uranium.

Finding the magnitude of the suppression is more involved. When $E_\gamma \ll E_e$, the photon $dN/dE \sim 1/\sqrt{E_\gamma}$, in contrast to the $1/E_\gamma$ Bethe-Heitler spectrum. At larger photon energies, a more fully quantum-mechanical analysis is needed. Migdal used the densities of wave states and scattering theory to calculate cross sections for all photon energies. Unfortunately, his formulae are recursive and difficult to use. The calculations for E-146 use a noniterative approximation developed by Stanev and collaborators [4]. The magnitude of the LPM effect for 1 TeV electrons in uranium ($E_e \sim 1/2\ E_{LPM}$) is shown in Fig. 2.

John Bell has pointed out that the LPM effect conflicts with classical electromagnetism by requiring that total radiation from the electron decrease as the electron energy increases [5]. Bell repeated and confirmed Migdals calculations. He argued that the discrepancy between the classical and quantum mechanical calculations is resolved by an increased emission of high-energy photons, where the classical formula is clearly inappropriate. Although doubts have been raised about Bell's calculations [6], his comments demonstrate that the ideas underlying the calculations are of fundamental interest.

An analogous effect occurs for pair creation by a high-energy photon. As Fig. 1 shows, the two processes are closely related. In pair creation, the LPM energy threshold is determined by the lepton with the lower energy. Because of this, suppression of pair creation begins at much higher energies than does bremsstrahlung suppression.

II. THE LONGITUDINAL DENSITY EFFECT AND MAGNETIC SUPPRESSION

Although the LPM effect reduces the divergence of the low-energy-photon production cross section, it does not eliminate it, since dN/dE_γ still grows as $E_\gamma^{-1/2}$. Another effect, which occurs at very low photon energies, removes the divergence. At low enough photon energies, the phase shift due to the effect of the medium on the photon, taken over the formation length, can become significant, and introduce a destructive interference. This effect is called the longitudinal density effect. In particle language, this phase shift occurs because the emitted bremsstrahlung photons undergo coherent forward Compton scattering off the electrons in the medium.

In classical electromagnetic language, the phase shift is due to the dielectric effect of the medium. The contributions to the photon amplitude, $\exp(i(k \cdot x - \omega t))$, from different parts of the electron path through the formation zone can interfere, and photon emission is suppressed [7]. This effect is related to the dE/dx (transverse) density effect discussed by Fermi. The density effect is significant for photon energies less than $\gamma\omega_p$, where ω_p is the plasma frequency. For a given material, this occurs at a fixed E_γ/E_e, and the suppression factor is [8]

$$\frac{\sigma_{density}}{\sigma_{no-density}} = (1 + \frac{nr_e\lambda_e^2 E_e^2}{\pi E_\gamma^2})^{-1},$$

where n is the electron density, r_e is the classical electron radius, and λ_e is the electron Compton wavelength. The density effect becomes important for $x = E_\gamma/E_e < 10^{-4}$ in lead, and 5.5×10^{-5} in carbon. Below these energies, $dN/dE_\gamma \sim E_\gamma^2$, removing the divergence.

In addition to disruption due to multiple scattering and dielectric effects, it is also possible for a magnetic field to suppress the bremsstrahlung. Magnetic suppression begins at an energy at which the bending due to the magnetic field, taken over the formation zone length, is larger than the bremsstrahlung emission angle $1/\gamma$. This happens for photon energy fractions $x < 2\gamma B/B_c$ where B_c is the critical magnetic field, $m_e^2c^3/e\hbar = 4.4 \times 10^{13}$ Gauss [9].

III. IMPLICATIONS OF THE LPM EFFECT

The LPM effect is relevant in a wide variety of physics applications. One of the most obvious applications is in calorimeters designed to study TeV particles, for example at TeV Linear Collider (TLC), Large Hadron Collider (LHC), or Next Linear Collider (NLC). All of these colliders can produce multi-TeV electrons, for which the LPM effect is large. Figure 2 shows one example, comparing the LPM and BH cross sections for a 1 TeV electron in uranium. The area under the energy-weighted cross-section curve is inversely proportional to the radiation length; it increases by about 5% due to the LPM correction. However, the major change is an increase in granularity of the showers, due to suppression of low-energy photons which would fill out the showers. This makes electromagnetic showers appear more like hadronic showers, reducing electron-hadron separation. For example, electrons may mimic pions in tau decays. Unfortunately, no calorimeter design studies include the LPM effect; the effect is omitted from both EGS and GEANT, although suppression due to dielectric effects is included in GEANT, but labeled as the Migdal effect. Analogous effects can occur in beamstrahlung [10].

The effects of LPM suppression on cosmic ray air showers have been discussed by many authors [11]. In exceedingly high-energy (above 10^{18} eV) photon-induced air showers, the LPM effect increases the graininess of the shower, and changes the shower particle density distribution used in determining total shower energy. Current air shower

detectors are insensitive to this effect, but future detectors will be more sensitive. Another potential impact occurs for electromagnetic showers from high-energy ν_e as might be produced by active galactic nuclei, and be observed by DUMAND [12].

The electronic LPM effect has a number of analogs in nuclear physics involving quarks and gluons moving through matter. Just as the original LPM effect predicts that photon emission from electrons traveling through dense charged matter can be suppressed, the nuclear analog predicts that gluon emission from quarks and gluons traveling through dense nuclear matter will be suppressed. Although the nuclear length scales are small, the elastic-scattering cross section is large, so the suppression is large. Brodsky and Hoyer have recently derived limits on color dE/dx, using formalisms similar to those used in LPM papers [13]. However, all analyses of QCD analogs are complicated by the strong-coupling nature of QCD, which makes interpretation of the data less than straightforward.

Another system in which LPM-type suppression appears is stellar interiors. Because the particles are nonrelativistic, it is easier to think temporally, comparing the Heisenberg emission times, calculated via the energy transfer with the average time between collisions. Because the density is very high, collisions are very frequent, leading to suppression of particle emission by nuclear bremsstrahlung. Raffelt and Seckel have shown that because the nucleon collision rate Γ_{coll} far exceeds the oscillation frequency of neutrino or axion radiation [14], production of these exotic particles is suppressed, and a number of existing limits will need to be reexamined.

IV. PREVIOUS EXPERIMENTS

A number of previous experiments have attempted to study the LPM effect and dielectric suppression. Except for a 1975 Soviet experiment, all of the LPM studies have used cosmic rays.

Most of the cosmic ray experiments were performed during the 1950s [15], with a few more recent results [16]. Most have looked at the depth of pair conversion in a medium for high-energy photons. They qualitatively confirmed the LPM effect, but with very limited statistics.

An experiment at Serpukhov [17] using 40 GeV electrons, was troubled by limited statistics, large systematic errors, and muon background, and so only produced a qualitative agreement with the LPM theory. The electrons transited a thin target, were bent by a magnet, and disposed of. A NaI crystal detected 20–80 MeV bremsstrahlung photons. The experiment suffered from large backgrounds, including bremsstrahlung in the air around the target and in the defining scintillation counters, debris from electrons hitting beam pipe walls, and synchrotron radiation.

Most of the experiments that have reported results on dielectric suppression were done by an Armenian group using electrons in the 1 GeV range to generate $\sim$ 100 keV photons. The experiments were optimized for transition radiation, but they have reported some results with solid targets, albeit of mixed quality [18].

Our experiment followed the general model of the Soviet LPM experiment but differed in almost all the particulars, to avoid the backgrounds that caused them trouble, and to measure several additional facets of the LPM effect.

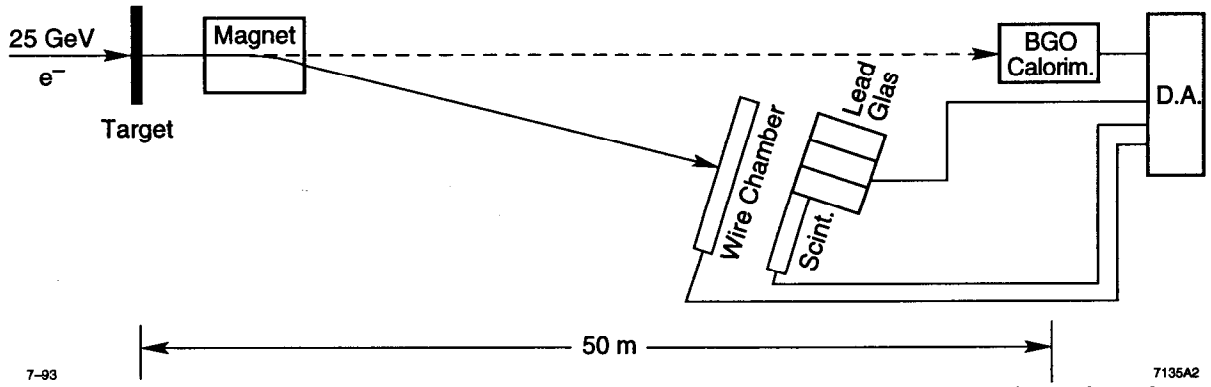

FIG. 3. The layout of SLAC-E-146. Electrons entering End Station A traversed a thin target and were bent downward by a bending magnet into a set of wire chambers and a lead glass block array. Bremsstrahlung photons emitted in the target continued downstream into a BGO calorimeter.

V. EXPERIMENTAL APPARATUS

Figure 3 shows a diagram of our experiment [19]. A 25 GeV electron beam enters Stanford Linear Accelerator Center (SLAC) End Station A and passes through a thin target. The beam is then bent downward by a 3.25 T-m dipole magnet, through six wire chamber planes which measure its momentum, and into an array of lead glass blocks which accurately count electrons. Produced photons continue downstream 50 meters into a BGO calorimeter array. To minimize backgrounds, the electron path visible to the calorimeter and the photon flight path are kept in vacuum.

A. Targets

The targets used are shown in Table 1. We used materials of a variety of densities and atomic numbers. The thicknesses chosen were a compromise between minimizing multiple photon emission from a single electron traversing the target, and maximizing the bulk LPM emission compared to edge effects. For most of the target materials, we used two targets with differing thicknesses. This allows a check on thickness-dependent effects, and for the possibility of removing edge effects by spectrum subtraction.

The targets were held in a seven-position target holder. During data acquisition, we cycled through the targets, typically changing targets every two hours. One position in the holder was always kept empty to allow us to take no-target background data. Another held a 1-cm-square silicon diode. The diode was sensitive to minimum ionizing particles, and was used periodically to measure the beam size and position.

B. Calorimeter

The BGO calorimeter, built in 1984 [21], is composed of 45 crystals in a 7 by 7 array with missing corners; each crystal measures 2 cm square by 20 cm (18 X_0) deep. This segmentation provides excellent position resolution, which is useful in separating synchrotron radiation from bremsstrahlung photons. The calorimeter response was studied previously with 40–100 MeV electrons at the Monterey Naval Postgraduate School Linac and with 1–8 GeV electrons

TABLE I. Targets Used in E-146. The gold targets were intended mainly to allow us to study very thin targets. The LPM energy is the highest energy for which LPM suppression is significant in the given target material.

Target Material	Z	X_0 (cm)	Thickness (X_0)	LPM Energy (MeV)
Carbon	6	18.8	2%, 6%	4.4
Aluminum	13	8.9	3%, 6%	9.2
Iron	26	1.8	3%, 6%	47
Tungsten	74	0.35	2%, 6%	235
Gold	79	0.34	0.1%, 1%, 6%	240
Lead	82	0.56	2%	147
Uranium	92	0.32	3%, 5%	265
Blank	-	-	-	-

at SLAC. These data were used to estimate the calorimeter nonlinearity (2%). Since BGO light output is known to change with temperature, we monitored the temperature throughout the experiment, and will use this data to correct for temperature drifts.

For this experiment, we used a number of methods to recalibrate the calorimeter, to obtain both an absolute energy calibration and a crystal-to-crystal intercalibration. The primary tools for measuring the relative gain were cosmic-ray muons, selected by a scintillator paddle trigger. Nearly vertical cosmic rays were selected, and the gain in each crystal was adjusted to produce equal signals.

The primary method for obtaining the absolute calorimeter gain was to run 400 and 500 MeV electron beams directly into the calorimeter. This calibration can be checked by comparing the electron energy loss, measured by the wire chamber, with the energy measured in the calorimeter. Because of the steeply falling photon spectrum and the non-Gaussian errors in the momentum measurement, this is a difficult measurement, but is useful as a check.

At very low energies, we took calibration data with a ^{60}Co source, which emits photons in pairs, with energies of 1.173 and 1.333 MeV. A scintillator triggered on one of the photons, providing an unbiased trigger for the other photon to interact in the BGO.

At this point, we estimate that the calorimeter calibration is accurate to 10%. In the future, this error should be roughly halved.

C. Spectrometer

The 18D72 bending magnet and the wire chambers formed a spectrometer which measured the momentum of the outgoing electrons. The 3.25 T-m field bent 25 GeV electrons downwards by 39 mrad, or 58 cm at the wire chambers, which were 15 meters downstream. The six wire chamber planes had a 2 mm wire spacing. Four of the planes provided y (momentum) information and the other two planes were angled to provide side to side positional information. With the 2 mm wire spacing and the 15 meter lever arm, we achieved a 100 MeV energy resolution, adequate to suppress many types of backgrounds, and to help calibrate the calorimeter.

D. Beam

The experiment required a beam intensity of about 1 electron per pulse. Because it would be very uneconomical to run the SLAC linac to produce a single electron per pulse, we devised a method to run parasitically during SLC/SLD operations, by using the particles that SLC throws away [20].

To do this, we took advantage of the roughly 10% of the SLC beam that, during normal operations, is scraped away by the collimators in sectors 29 and 30 of the SLAC linac. Because the collimators are only 2.2 X_0 thick, a usable flux of high-energy photons emerges from the back and sides of the collimator. A small fraction of these photons travel down the beampipe, past the magnets that bend the electrons and positrons into the SLC arcs, and into the beam switchyard. There, we placed a 0.7-radiation-length target to convert these photons into e^+e^- pairs. A fraction of the produced electrons were captured by the A-line optics and transported into the end station.

Although it sounds like a Rube Goldberg contraption, this process worked extremely well, and the beam size, divergence, and yield matched our simulations. At 8 and 25 GeV, the beam intensity was in the 1–100 electrons/pulse range. To minimize the spot size in the calorimeter, the beam optics were adjusted to produce a virtual focus at the calorimeter; photon spot sizes there were typically a few mm in diameter. The beam spot was stable enough and small enough that beam motion was not a problem.

VI. DATA ANALYSIS AND RESULTS

This analysis will only consider events containing a single electron. While multiple electron events can be used to study systematic effects and improve the statistics, their analysis is more involved and will not be discussed here. Single electron events were selected by requiring that the energy deposition in the lead glass blocks match that for a single electron, with no energy deposited in the veto counters which detected lower energy electrons. The photon energy was found by summing the energies of hit BGO crystals using a cluster-finding algorithm. The cluster finding reduced the noise level by eliminating random hits. The energies were histogrammed logarithmically using 25 bins per decade of energy, so that each bin had width $\Delta E \sim 10\% E$. The logarithmic binning was chosen because a $1/E_\gamma$ BH spectrum will have an equal number of events in each bin, simplifying the statistical analysis.

A. Backgrounds and Monte Carlo

The backgrounds to the LPM measurement were small. The major background-related correction is for multi-photon pileup, when a single electron emits two bremsstrahlung photons while traversing the target. This correction is accounted for in the Monte Carlo simulation.

The Monte Carlo tracked electrons through the material in small steps, allowing for the possibility of bremsstrahlung in each step. It used the formalism developed by Stanev and collaborators [4] to avoid the recursion in the formulas developed by Migdal. However, numerical tables of Φ and G given by Migdal were used, rather than the series given by Stanev. The longitudinal density effect was included by a simple multiplicative factor [8]. Either the LPM or longitudinal density effects could be turned off as needed. By choice, and for consistency, our BH Monte Carlo results were obtained by turning off the LPM effect, but otherwise using Migdal's formulae, rather than newer formulae that

include some subtle corrections. Because we are in the region of complete nuclear screening, these corrections are small.

Produced photons can either exit the target or be lost by Compton scattering or pair conversion, according to tabulated probabilities [22]. Because of the low probabilities, large production angles, and small sensitive solid angles, bremsstrahlung from secondary electrons from pair conversion have a negligible effect on our data. Finally, although it is a small effect, our Monte Carlo includes a simple model of the calorimeter resolution.

Background sources included synchrotron radiation, transition radiation, and photonuclear interactions. Synchrotron radiation from both the final A-line bending magnet and our spectrometer magnet were considered. The good photon positional resolution provided by the BGO calorimeter allowed us to identify most synchrotron radiation by positional cuts. Because of the large fringe field of the spectrometer magnet, the electron bend began very gradually, and synchrotron radiation reaching the calorimeter came from low field regions. Because of this, synchrotron radiation hitting the center calorimeter crystal came from regions with a maximum critical energy of 100 keV.

Transition radiation as electrons enter and leave the target, is also very small, amounting to an average of 14 keV per electron, with the photon spectrum extending only up to $\gamma\omega_p$, the same energies at which the longitudinal density effect occurs [23]. So, this background is negligible above 5 MeV.

The photonuclear cross section is a small fraction of the bremsstrahlung cross section. In addition, the chance of a photonuclear interaction mimicking bremsstrahlung in our detector is very small, so photonuclear interactions should have negligible effect on our data.

The non-target-related backgrounds were checked by taking data with an empty target holder. This showed that our backgrounds were indeed very low, typically 0.1% of a photon per electron. Compared with the 20–60% per electron chance of a bremsstrahlung photon, it is clear that the non-target-related backgrounds are indeed small.

Most possible target-related backgrounds should distribute photons all over the calorimeter, in contrast to bremsstrahlung, which should be concentrated in the center. The observed paucity of hits away from the central region indicates that target related backgrounds are also small.

B. Results

We present our results in comparison with two Monte Carlo calculations, one for the BH spectrum and the other including the LPM and longitudinal density effects. Figure 4 compares the result of our calculations with the data for 2% X_0 and 6% carbon radiators. The dashed line on the 2% plot shows the raw BH cross section; multiphoton pileup is a large effect even for the relatively thin targets. The two spectra differ below about 10 MeV; the data shows a downturn which matches the LPM spectrum. In this and successive plots, we have adjusted the normalization to match the data. For 2% carbon, this was a 6% adjustment; for the other samples the normalization adjustment is between 3% and 7%; this is within the range of our systematic errors.

The LPM effect is much more significant in denser, high Z targets. Figure 5 shows the bremsstrahlung spectrum for 25 GeV electrons traversing 3% and 5% uranium targets. The spectrum agrees well with the LPM Monte Carlo

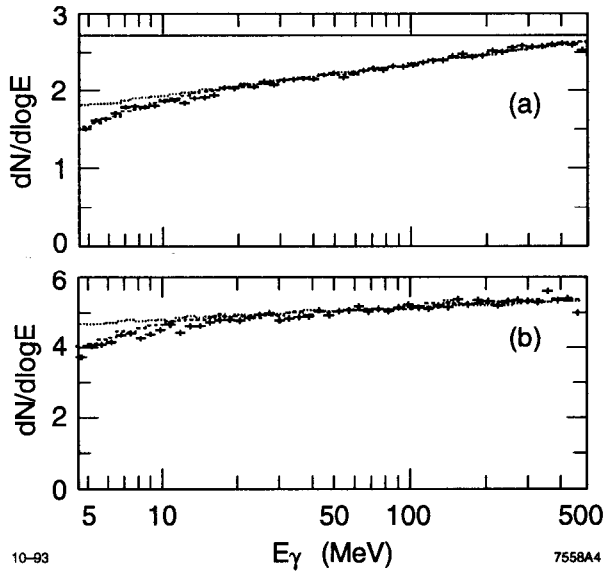

FIG. 4. The bremsstrahlung spectrum, $d\sigma/d\log(E)$ data (crosses), compared with the LPM (dashed histogram) and BH (dotted histogram) Monte Carlos, for (a) 2% and (b) 6% X_0-thick radiators of carbon. The cross section units are photons per bin (with 25 bins per decade) per 1000 electrons. The solid line in (a) shows the BH cross section neglecting multi-photon effects.

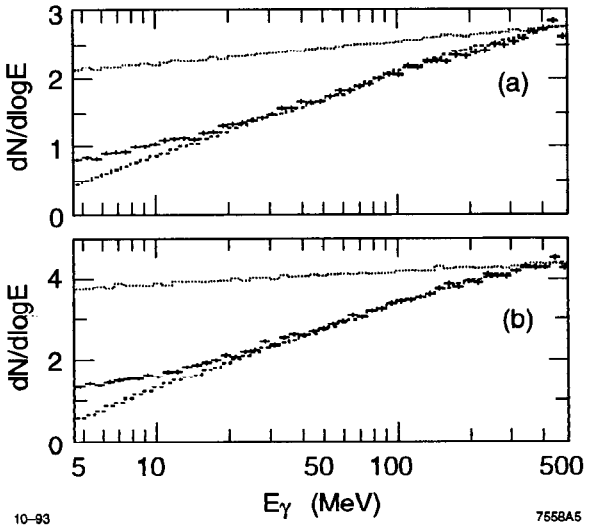

FIG. 5. The bremsstrahlung photon spectrum for 25 GeV electrons traversing (a) 3% and (b) 5% uranium radiators. The dotted histograms are the BH Monte Carlo, the dashed histograms the LPM Monte Carlo, and the crosses are data.

down to about 25 MeV, while the BH curve is clearly ruled out. Below 25 MeV, the data is significantly higher than the Monte Carlo. This is because of edge effects as the electron enters and leaves the target.

C. Thin Targets and Edge Effects

If an electron radiates near the target edge, the formation zone can extend outside of the target, where there is no multiple scattering. Then, less LPM suppression occurs.

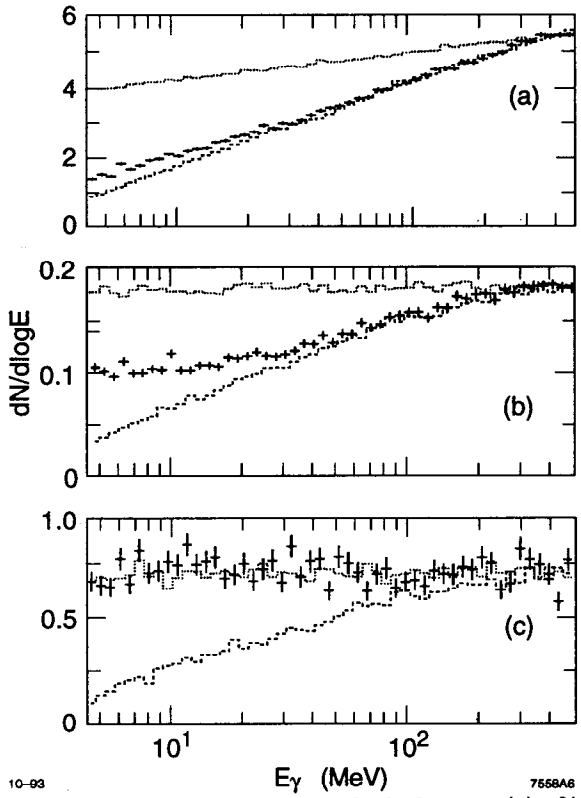

FIG. 6. The bremsstrahlung spectra for three gold targets with thicknesses (a) 6% X_0, (b) 1% X_0, and (c) 0.1% X_0. The dotted histograms are the BH Monte Carlo, the dashed histograms the LPM Monte Carlo, and the crosses are data. As the target becomes thin compared to the formation zone length, LPM suppression disappears and the BH spectrum reappears.

For very thin targets, where the multiple scattering angle, taken over the entire target thickness is less than $1/\gamma$, LPM suppression should not be present, and a BH emission spectrum should be seen. For thicker targets, one might expect an 'edge effect' to account for scattering near the material boundaries, with the bulk material retaining the LPM spectral emission.

Because the formation zone length scales as E_e^2/E_γ, these effects should be photon energy dependent. However, it should also be noted that the formation zone has a maximum length limited by the longitudinal density effect.

The absence of LPM suppression in thin targets and the appearance of edge effects can be explored by comparing spectra from three gold targets, one quite a bit thicker than the formation zone length at these energies (6% X_0, or 200 μm), one comparable to the formation zone length at 30 MeV (1% X_0, or 30 μm), and one much thinner than the formation zone length over the 5–500 MeV range (0.1% X_0, or 3 μm).The spectra for these targets are shown in Fig. 6.

Gol'dman [24] studied this problem theoretically; unfortunately he did not present his results in closed form. Later, Ternovskii [25] extended his treatment, and gave clear formulae. Both authors described a sort of transition radiation to mark the change in the electron's forward velocity, as it changes from a straight trajectory to being scattered by collisions with the atoms in the target media. This is intended to be analogous to the more traditional transition radiation. Unfortunately, Ternovskii's formulae are unphysical, and predict transition radiation far in excess of the discrepancies shown in the data.

We can partially bypass these edge effects and measure the bulk LPM effect by subtracting the spectra of two targets of the same material but differing thickness. Figure 6 shows the difference between the 5% and 3% uranium target

TABLE II. Summary of Systematic Errors in the E-146 LPM Measurement. The effects of the errors are given in terms of their affects on the absolute and relative cross section measurements. The absolute cross section measurement is taken at 500 MeV, while the relative σ is the amount that the cross section can change at other energies, relative to the 500 MeV point. The calorimeter calibration and cluster finding entries show the amount that the allowed energy shifts could affect the cross section measurement for the 5% uranium target. Other targets will have similar or smaller shifts. For conservatism, and since several of these errors are clearly non-Gaussian, the errors are added linearly here.

Source	σ(500 MeV)	σ(Relative)
Backgrounds		1%
Calorimeter Calibration (10%)	2%	2.5%
Cluster Finding (10%)		2.5%
Target Thickness	2%	
Target Density		2%
e^- flux	3%	
Monte Carlo	1%	3%
Subtraction		8%
Sum	8%	19%
Migdal Formulae	5%	5%

spectra, properly normalized to account for the number of electrons impacting each target. With this subtraction, the data agrees well with the LPM Monte Carlo down to 15 MeV; below 15 MeV the data is slightly higher than the Monte Carlo. The BH prediction is clearly excluded.

The disagreement with the LPM Monte Carlo is due to an offset introduced by the subtraction procedure. While the Monte Carlo accounts for multiphoton emission, it does not include the additional multiphoton emission due to the transition radiation. Thus, the subtraction procedure removes the transition radiation, but undercompensates for the multiphoton emission, and predicts a smaller cross section than the data. In the future, we plan to fit the edge effects numerically and include them in the Monte Carlo. For the present analysis, it is difficult to predict the magnitude of the correction, but it is not inconsistent with the currently observed discrepancy.

D. Systematic Errors

The major systematic errors come from backgrounds, uncertainties in the electron flux, target thickness and density, Monte Carlo accuracy, calorimeter calibration, and calorimeter cluster finding. Our preliminary estimates of these systematic errors are summarized in Table 2.

We have divided the cross section errors into two parts: absolute and relative. The absolute part applies to a measurement of the cross section at 500 MeV, the energy at which we calibrated the calorimeter with an electron beam. The relative part refers to how much the cross section changes across the 5 to 500 MeV range. So, the relative cross section is relevant when considering the shape of the curve.

As previously discussed, the major backgrounds are synchrotron radiation, transition radiation, and nuclear interactions in the target. These backgrounds can only affect the low energy end of the spectrum.

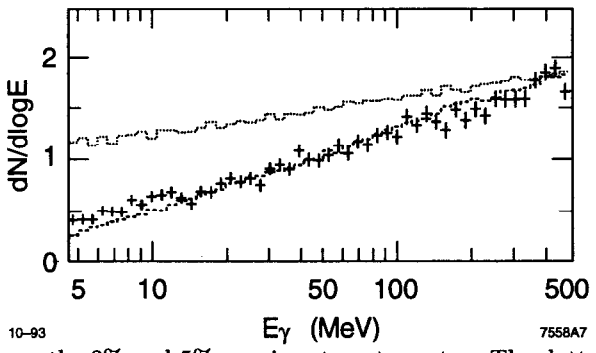

FIG. 7. The difference between the 3% and 5% uranium target spectra. The dotted histogram is the BH Monte Carlo, the dashed histogram the LPM Monte Carlo, and the crosses are data.

The calorimeter calibration uncertainty of 10% is equivalent to shifting the histogram contents sideways by one bin. The energy uncertainty affects the cross section measurement with a magnitude depending on the slope of the curve $d\sigma/d\log(E_\gamma)$; for the 5% X_0 uranium target, it contributes a 2.5% uncertainty in the cross section. Any errors in the cluster finding, either the inclusion of stray noise, or the omission of valid energy, will have a similar effect, but concentrated at the low end of the spectrum.

We measure the target length, width and mass, to find the thickness in g/cm^2, to 2% accuracy. Finding the actual density is less straightforward. Graphite can vary significantly in density; for the carbon targets we actually measured their thickness, to find their density, with an estimated 5% systematic error. The uranium targets are too thin and malleable to allow for an accurate thickness measurement; we assign a 1% systematic error to account for natural density variations. The thickness mainly affects the absolute normalization, while the density affects the size of the LPM suppression.

We believe that we know the electron flux to 3% at this point.

The Monte Carlo should represent the Migdal formulae within 3%, with most of the inaccuracy coming from the use of interpolations to the data points calculated by Migdal. This can be reduced in the future by using better approximations [4].

These errors are large enough to account for the difference in normalization between the data and Monte Carlo discussed in the previous sections. When the effects of multiphoton pileup in the subtraction procedure are included, they are large enough to account for the discrepancy in Fig. 7 at low energies.

It is worthwhile to briefly discuss the accuracy in Migdal's calculation. Migdal uses a Fokker-Plank expansion to solve his differential equation. This approximation introduces an error of unknown size. We can, however, get one hint about his final accuracy by looking at his equations in the limit of no suppression; they should then match the BH formulae. Indeed, his equations do match BH to logarithmic accuracy. More quantitatively, for large photon energies, they agree to within 5%.

E. Longitudinal Density Effect

In addition to the data described above, we took some data with the calorimeter gain increased by roughly a factor of 10. This allowed us to study the bremsstrahlung spectrum down to 500 keV, where the longitudinal density effect introduces a large suppression. Because the longitudinal density effect is far less X_0 sensitive than the LPM effect,

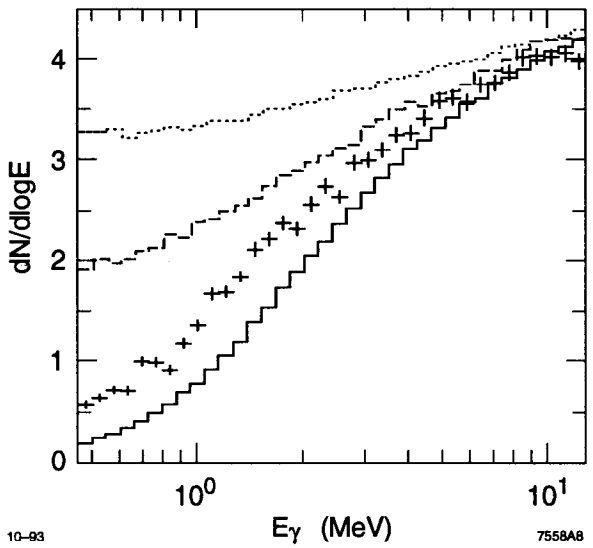

FIG. 8. Bremsstrahlung photon spectrum from 6% X_0thick carbon target, in the energy range 500 keV to 10 MeV. Shown are three Monte Carlo results, BH (dotted histogram), LPM only (dot-dashes), and LPM with dielectric suppression (dashes), in addition to the data(crosses).

longitudinal density suppression can be seen most clearly in light targets, so we will concentrate here on the carbon targets.

Before proceeding, it is worthwhile to point out that the experimental conditions are significantly different from those at higher energies. The experimental backgrounds, especially synchrotron radiation, are quite large. The calorimeter functions quite differently, with the dominant energy loss being by Compton scattering, with most of the energy confined to a single crystal. In contrast, at higher energies, loss is via pair production and electromagnetic showers, which spread over a larger region. These conditions call for different data analysis strategies to reduce the backgrounds.

Most of the synchrotron radiation from our spectrometer magnet occurs in a narrow strip downward from the center of the calorimeter. We can eliminate most of the it by requiring that the center of gravity of the calorimeter energy cluster be above the midpoint of the calorimeter. Also, because of the smaller energy deposition size, tighter cluster cuts were used in the analysis.

These cuts lead to Fig. 8, showing the spectrum from a 6% carbon target. Below 5 MeV, the data drops rapidly. Also shown for comparison are results from three Monte Carlo calculations: BH, LPM only, and LPM with dielectric suppression. The data is between the LPM only and LPM with dielectric suppression results.

There are a number of possible reasons for the disagreement: remaining backgrounds, calorimeter effects, and other photon sources. The remaining backgrounds are the small remaining synchrotron radiation and transition radiation, which can become significant below 1 MeV.

The calorimeter and electronics response is complicated for small signals. Calorimeter and electronic noise become more significant. Random and synchronous noise was greatly reduced by using a 5 ADC count (50 keV here) on the calorimeter readout for each crystal. This had the undesirable effect of eliminating some of the crystals from the calorimeter signal. At the low end of the range, the calorimeter light output of 1 photoelectron per 10 keV became

problematic; The lower edge of Fig. 8, 500 keV, corresponds to 50 photoelectrons, so photoelectron statistics alone introduce a 14% uncertainty in the energy.

We are now evaluating these contributions in detail, but it is clear that there is significant suppression at low energies. As a check that it isn't entirely due to the LPM effect, we have studied some of the data taken with 8 GeV electrons. Because the LPM energy scales as the beam energy squared, whereas the minimum density suppression energy only scales as the beam energy, at 8 GeV LPM suppression should be minimal, but longitudinal density suppression should remain. This data shows that the falloff remains, and so should be due to the longitudinal density effect.

VII. CONCLUSIONS

We have measured the bremsstrahlung photon spectrum from 25 GeV electrons in thin targets of a variety of materials. For photons with energies of 5 to 500 MeV, the bremsstrahlung spectrum matches that predicted by Landau, Pomeranchuk, and Migdal. For very thin targets, the suppression is reduced or eliminated, as predicted by theory.

We see qualitative evidence for longitudinal density suppression.

A detailed analysis is in progress; we expect a final experimental precision of a few percent, matching the accuracy of the calculations.

ACKNOWLEDGMENTS

We are indebted to the SLAC management and staff for their enormous cooperation in performing this experiment. In particular, we would like to thank groups E, C, and EFD for their assistance in setting up the experiment and accelerator operations for their efficient beam delivery. Professor Walter Meyerhof graciously provided the target holder we used. We also acknowledge many useful conversations with Stan Brodsky and Pisin Chen.

---

[1] L. D. Landau and I.J. Pomeranchuk, Dokl. Akad. Nauk. SSSR **92**, 535 (1953); **92**, 735 (1953). These two papers are available in English in L. Landau, *The Collected Papers of L.D. Landau*, Pergamon Press, 1965.

[2] A.B. Migdal, Phys. Rev. **103**, 1811 (1956).

[3] E.L. Feinberg and I. Pomeranchuk, Nuovo Cimento, Supplement to Vol **3**, 652 (1956).

[4] T. Stanev *et al.*, Phys. Rev. **D25**, 1291 (1985).

[5] J.S. Bell, Nuclear Physics **8**, 613 (1958).

[6] M. Gyulassy has pointed out that, in the integral in the first equation in Section 3 of Bell's paper, the term $\delta(1-\cos\theta u)/t$ is omitted.

[7] M.L. Ter-Mikaelian, Dokl. Akad. Nauk. SSR **94**, 1033 (1954). For a discussion in English, see M.L. Ter-Mikaelian, *High Energy Electromagnetic Processes in Condensed Media*, John Wiley & Sons, 1972.

[8] W.R. Nelson, H. Yirayama, and D.W.O.Rogers, SLAC–Report–265, Dec. 1985. Unfortunately, after such a nice discussion they did not include the effect in EGS.

[9] V.N. Baier, V.M. Katkov, and V.M. Strakhovenko, Institute of Nuclear Physics preprint 87-26 (in Russian); V.N. Baier and V.M Katkov, Sov. Phys. Dokl. **17**, 1068 (1973); V.M. Katkov and V.M. Strakhovenko, Sov. J. Nucl. Phys. **25**, 660 (1977). The latter papers only apply to the case in which the transverse momentum is much less than m.

[10] Pisin Chen and Spencer Klein, in *Proceedings of the 3rd Intl. Workshop on Advanced Accelerator Concepts*, Port Jefferson, NY, June, 1992.

[11] E. Konishi *et al.*, J. Phys. G. **17**, 719 (1991). See recent (1970s–1990s) proceedings of the International Cosmic Ray Conferences.

[12] A. Misaki, Fortschr. Phys. **38**, 413 (1990); J. G. Learned and T. Stanev, in Proc. 3rd Intl. Workshop on Neutrino Telescopes, Venice, Italy, Feb., 1991.

[13] S. Brodsky and P. Hoyer, Phys. Lett. **B298**, 165 (1993).

[14] G. Raffelt and D. Seckel, Phys. Rev. Lett. **67**, 2605 (1991).

[15] P.H. Fowler *et al.*, Phil. Mag. **4**, 1030 (1959).

[16] S.C.Strausz *et al.*, in *Proc. 22nd Intl. Cosmic Ray. Conf.*, Dublin, Ireland, 11–23 Aug, 1991.

[17] A. Varfolomeev *et al.*, Sov. Phys. JETP **42**, 218 (1976).

[18] F.R. Arutyunyan, A.A. Nazarayan, and A.A. Frangyan, Sov. Phys. JETP **35**, 1067 (1972).

[19] M. Cavalli-Sforza *et al.*, SLAC–Proposal–E146, June, 1992.

[20] L. Keller *et al.*, to be submitted to IEEE Trans. Nucl. Sci.

[21] I. Kirkbride, in the SLAC Users Bulletin No. 97, Jan.–May 1984, pg. 10–11.

[22] J. Hubbell, H. Gimm, and I. Overbo, J. of Physical and Chemical Reference Data **9**, 1023 (1980).

[23] J.D. Jackson, *Classical Electrodynamics, 2nd edition*, John Wiley & Sons, 1975.

[24] I.I. Gol'dman, Sov. Phys. JETP **11**, 1341 (1960).

[25] F.F. Ternovskii, Sov. Phys. JETP **12**, 123 (1960).